Iran University of Science and Technology

International Journal of

Railway Research

Dynamic Scaling of Train-Track-Bridge Models: Sensitivity Analysis and Dimensional Considerations

M. Soltanzadeh[1], T. Bahri[1], M.A. Rezvani[1*]

[1]School of Railway Engineering, Iran University of Science and Technology, Tehran, Iran

ARTICLE INFO

Article history:
Received: 11.05.2024
Accepted: 22.12.2024
Published: 23.12.2024

Keywords:
Vehicle Dynamics
Dynamic Scaling
Train/Track/Bridge Structures
Damage Identification
2D Modeling

A B S T R A C T

This study examines the dynamic scaling of train-track-bridge interaction models, focusing on the sensitivity of the Train-Track-Bridge Dynamic Interaction (TTBDI) system to changes in primary dynamic identifiers. Utilizing the MATLAB TTB-2D code, this research investigates the vibrational behavior of scaled models, which is crucial for damage detection without compromising actual structures. This study establishes scaling relationships for primary and secondary identifiers, with the correlation coefficient acting as the key indicator of similarity between real and scaled responses. Sensitivity analysis demonstrates that the TTBDI system's response is highly sensitive to changes in mass and stiffness scales, while less affected by variations in length and damping coefficient scales. Additionally, this work introduces a relationship for the dynamic scaling of the TTBDI system. The effectiveness of this method is then numerically examined. It is observed that the real and scaled responses will align, confirming that scaling is correctly performed. The investigations conducted in this research aim to increase accuracy in constructing dynamic scaled devices for trains, tracks, and bridges, enabling feasibility studies for system damage identification.

1. Introduction

In recent years, extensive research has been conducted in the field of dynamic interaction between trains, bridges, and tracks. Some of these studies have constructed a laboratory-scaled dynamic model of a train and bridge to verify the accuracy of the results. The advantages of using laboratory-scaled dynamic models include:

- A laboratory-scaled dynamic model is required to investigate the vibrational behavior of bridges with damage, as creating actual damage in real bridges is not feasible.
- Training neural networks to detect damages requires repeated experiments of train passage over the bridge. With suitable dynamic model, neural networks can be trained more rapidly.

The following will provide an overview of the research conducted with laboratory-scaled dynamic models.

Lin *et al.* (2005) pioneered this field by using a motor-pulled cart equipped with an accelerometer to induce and measure vibrations on a bridge, using Fast Fourier Transform (FFT) for analyzing the data to determine the bridge's dynamic properties [1].

In 2012, F. Cerda *et al.* advanced the field by validating an indirect monitoring method that utilized equipped vehicles and short-term Fourier transform to detect bridge failures, demonstrating accurate failure detection [2]. This approach was further enhanced by G. Lederman *et al.* (2014), who developed

*M.A. Rezvani
Email address: Rezvani_ma@iust.ac.ir

algorithms to detect damage severity and location using signal processing and machine learning, with experiments confirming the method's effectiveness [3]. In the same year, C.W. Kim *et al.* demonstrated a vehicle-based inspection method for short bridges, confirming its ability to identify damage location and severity [4], while F. Cerda *et al.* presented an indirect monitoring approach, proving its capability to detect various types of bridge damage using a laboratory-scaled model [5].

The feasibility of using a vehicle with an accelerometer to monitor bridge dynamics was shown by McGetrick *et al.* (2015), although they did not make scaling comparisons [6]. This gap was addressed by subsequent studies, such as those by W. Zhang *et al.* (2017), who proposed a fault identification approach without a model, using phase paths and a fault index, with laboratory experiments supporting its success [7]. Yang *et al.* and S. Urushadze *et al.* (2017) proposed and tested an indirect frequency approach, recording bridge frequencies from a vehicle's motion, proving the method's feasibility [8]. C. Kim *et al.* (2017) compared direct sensor-based and mobile vehicle-based inspection methods, with laboratory experiments showing practicality [9].

The research continued to evolve with Y. Lin *et al.* (2018) using semi-static influence lines for damage detection, with numerical and experimental data supporting the method's effectiveness [10]. Q. Mei *et al.* (2019) introduced a framework using smartphones in vehicles as sensors, with experiments showing successful damage identification and potential for real-time monitoring of multiple bridges [11]. This innovative approach leveraged the ubiquity of smartphones to facilitate widespread bridge monitoring.

Recent studies have further refined these methods. S. Zhang *et al.* (2019) utilized tensioned impact lines (ILs) for damage detection in bridges, confirming the method's effectiveness through experiments on a small-scale concrete bridge model [12]. Z. Zhau *et al.* (2019) utilized the DVV method with acceleration measurements to identify bridge damage, validating the method's feasibility for simple supported concrete bridges [13]. J. Li *et al.* (2019) proposed identifying bridge modal parameters using single-channel blind analysis, with laboratory tests successfully extracting modal frequencies [14].

In 2020, the field saw significant advancements with Z. Nie *et al.* introducing a damage detection approach for deck bridges using two sensors, and L. Zhang *et al.* developing a method for damage identification in simply supported bridges using sensors, achieving high accuracy in both damage and load identification [15]. S. Pourzeynali *et al.* extended existing methods to identify moving loads on bridges, demonstrating the method's insensitivity to sensor placement and sampling frequency [16]. J. Zhang *et al.* proposed a momentary frequency identification method using the modified S-transform technique, showing improved detection of momentary frequency and better performance in bridge health monitoring [17].

D. Cantero *et al.* (2019) investigated frequency changes in vehicle-bridge systems due to vehicle position, revealing different frequency changes and highlighting the influence of mechanical properties beyond mass [18]. S. Pourzeynali *et al.* (2020) extended existing methods to identify moving loads on bridges, demonstrating the method's insensitivity to sensor placement and sampling frequency [19]. J. Zhang *et al.* (2020) proposed a momentary frequency identification method using the modified S-transform technique, showing improved detection of momentary frequency and better performance in bridge health monitoring [20].

Based on the reviewed articles, the scaling of the constructed system and the alignment of results with the actual dynamic models of trains and bridges have not been examined. The reason is that each of the conducted experiments has been designed for feasibility and validation of a specific method, most of which are related to the identification of bridge damages. However, dynamic scaling of the vehicle and bridge is only accurately performed when the results can align with the actual dynamic model. This can improve the precision and credibility of the proposed methods in determining bridge damages.

2. Numerical simulation and introduction of TTBDI system

The purpose of this study is to investigate the impact of various dynamic quantities on the dynamic scaling of train and bridge models for constructing laboratory samples. Conducting these studies before designing and building a scaled model is essential to identify the important and influential parameters in scaling. By examining the impact of these parameters, it can be determined that how each dynamic parameter affects the final response and the extent of deviation between the scaled model's response and the actual model. To examine signal behaviors, the correlation coefficient will be calculated.

TTB-2D is a MATLAB code that solves the problem by setting the dynamic parameters associated with the train-bridge system and the initial and boundary conditions. This code can provide displacement, velocity, acceleration, force, and torque responses in different degrees of freedom of train or bridge elements [21,22]. Numerical modeling of TTB-2D in this article is used to simulate the dynamic interaction problem of the train and the path and bridge. In [23], a direct comparison between a 2D TTB model and a 3D model showed that the 2D model could predict the vertical dynamic behavior of the system with sufficient accuracy. The train is represented as a sequence of separate wagons. Each wagon has been modeled using the mechanical model proposed for train-bridge interaction by the European Railway Research Institute [24]. According to Figure 1, the main body is connected to two bogies, each with two axles connected by primary suspension. The motion equations for the vehicle are simplified to a system with 6 degrees of freedom (DOF) [25]. TTB-2D provides various types of trains and vehicle configurations from different sources listed in Table 1. Using these examples, the desired train configurations can be created. Rail roughness is defined as a spectral feature based on random samples. These samples can be taken from real experiences or previous simulations. However, in this article, the wheel-rail contact is considered without roughness and completely smooth. In the TTB-2D model, the rail and bridge are represented as Euler-Bernoulli beams, and other parts of the railway are modeled as concentrated mass elements. Therefore, TTB-2D is an accessible implementation of the train-rail-bridge interaction problem based on published formulas and methods. Finally, all model details are converted into a combined system, and the motion equations for the train and infrastructures are interconnected [26].

Figure 1 represents the general dynamic modeling of the train, path, and bridge. The stiffness and damping coefficients of the pads between the rail and sleepers, the concentrated mass of sleepers, the stiffness, damping, and mass coefficients of the ballast, and the stiffness, damping, and mass coefficients of the sub-ballast are repeated at specific intervals from each other. The bridge is modeled as an Euler-Bernoulli beam with adjustable support conditions that can be fixed or defined with stiffness coefficients in vertical and rotational directions. In this study, the supports are assumed to be fixed [21,22].

Figure 2 presents the dynamic model of the train with six degrees of freedom. The train consists of three main concentrated masses (m, m_B1, m_B2), one of which is the mass of the wagon and the other two are the masses of the bogies. Each mass has one degree of freedom in the vertical direction and one degree of freedom in the rotational direction. The wheels are represented by four specific masses whose contact with the rail is inseparable. The primary suspension is modeled by spring and damper elements between the wheels and bogies, and the secondary suspension is modeled by spring and damper elements between the bogies and the wagon. The selected train model is the Manchester Benchmark passenger train, and its dynamic and geometric information is provided in Table 2 in the appendix. It is assumed that the train passes over the rail and bridge at a speed of 10 meters per second, and the contact between the wheels and the rail is inseparable and without roughness. The bridge supports are fixed in the vertical direction and free in the rotational direction. In addition, the dynamic and geometric information of the rail and bridge is provided in Table 3 in the appendix [21,22].

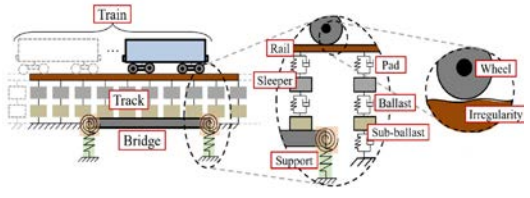

Figure 1 Dynamic modeling of the train, track, and bridge in general [21]

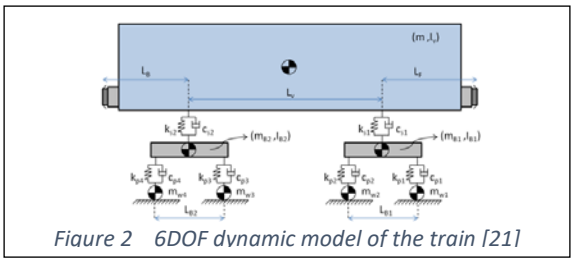

Figure 2 6DOF dynamic model of the train [21]

Table 1. Train model and source of identifiers.

Train type/configuration	Reference
Manchester Benchmark	[6]
ICE3 Velaro	[7]
Chinese Star Power Car Double Deck Passenger Coach	[8]
Eurostar	[9]
Pioneer M and R vehicles	[10]
Shinkansen S300	[11]

3. Proposed assumptions

Dynamic scaling of trains, tracks, and bridges is fully achieved when the response of the TTBDI system components to real inputs is completely identical to the system's response to scaled inputs. A classification is assumed for quantities in scaling, dividing them into real quantities and scaled quantities. In relationships, real quantities are indicated with index 1 and scaled quantities with index 0. Another classification is also assumed for quantities, dividing them into two main categories: the primary and the secondary quantities are always influenced by the primary quantities and are related to them.

The scale of each quantity is equal to the division of the real value of the quantity by its scaled value. Relationships 1 to 4 are the scales of the primary quantities, and 5 to 9 are the scales of the secondary quantities.[27]

Length scale:

$$\emptyset_l = \frac{l_1}{l_0} \quad (1)$$

Mass scale:

$$\emptyset_m = \frac{m_1}{m_0} \quad (2)$$

Stiffness scale:

$$\emptyset_K = \frac{K_1}{K_0} \quad (3)$$

Damping scale:

$$\emptyset_C = \frac{C_1}{C_0} \quad (4)$$

Velocity scale:

$$\emptyset_V = \frac{\emptyset_l}{\emptyset_t} = \frac{\emptyset_l}{1} = \emptyset_l \quad (5)$$

Moment of inertia scale:

$$\emptyset_I = \frac{I_1}{I_0} = \emptyset_m * {\emptyset_l}^2 \quad (6)$$

Second moment of area scale:

$$\emptyset_j = \frac{j_1}{j_0} = {\emptyset_l}^4 \quad (7)$$

Mass per unit length scale:

$$\emptyset_{\boldsymbol{\mu}} = \frac{\boldsymbol{\mu_1}}{\boldsymbol{\mu_0}} = 1 \quad (8)$$

Modulus of elasticity scale:

$$\emptyset_E = \frac{E_1}{E_0} = 1 \quad (9)$$

The similarity of the TTBDI system's response to real input (real response) and the system's response to scaled input (scaled response) is essential in the dynamic scaling of this system. One of the most important criteria for determining the similarity of the two signals is the correlation coefficient. Equation (10) shows the calculation of the correlation coefficient between the two discrete signals. In this equation, X and Y are the two discrete signals, and R is the correlation coefficient between these two signals. The absolute value of the correlation coefficient is always a number between 0 and 1, and the closer it is to 1, the more similar the two signals are [28].

$$R = \frac{\sum_k X_k Y_k}{(\sum_k X_k)^{\frac{1}{2}} (\sum_k Y_k)^{\frac{1}{2}}} \quad (10)$$

This research has examined the sensitivity of the TTBDI system to changes in the scale of its primary quantities. The system's sensitivity criterion is the correlation of the two signals, real response, and scaled response. During construction, the precision of construction can be more focused on the quantities to which the system is more sensitive. For this research, the scale of each parameter is increased up to the value of 25

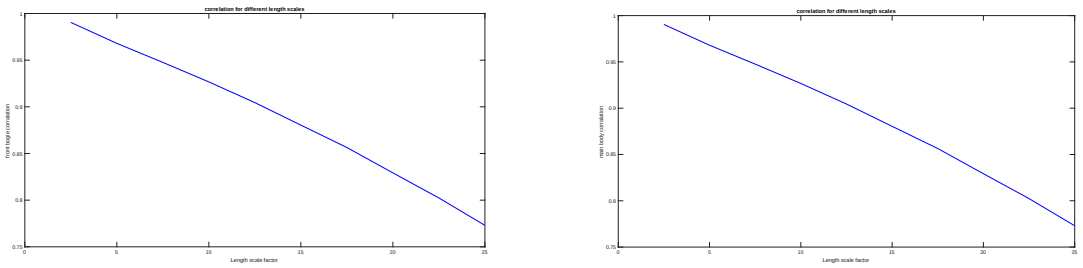

Figure 3 The impact of scaling length on the correlation coefficient of real and scaled responses in the acceleration signals of the front bogie and wagon.

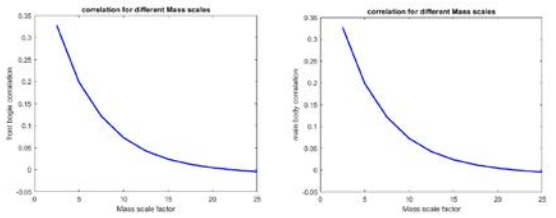

Figure 4 The impact of scaling mass on the correlation coefficient of real and scaled responses in the acceleration signals of the front bogie and wagon.

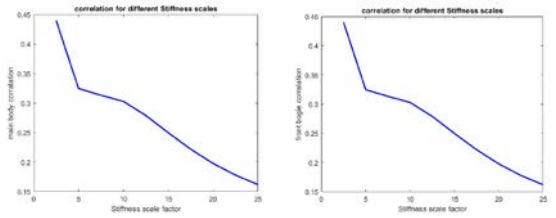

Figure 5 The impact of scaling stiffness on the correlation coefficient of real and scaled responses in the acceleration signals of the front bogie and wagon.

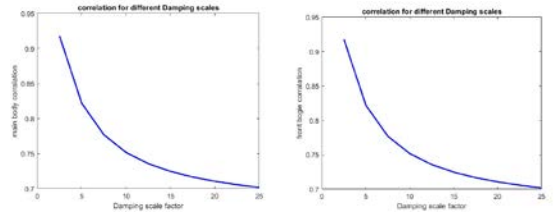

Figure 6 The impact of scaling the damping coefficient on the correlation coefficient of real and scaled responses in the acceleration signals of the front bogie and wagon.

with a step length of 2.5, and at each step, the correlation coefficient between the signals of the real response and the scaled response is recorded. These studies have been conducted on two responses: the vertical acceleration of the front bogie and the vertical acceleration of the wagon center. Figures 3 to 6 present the sensitivity analysis of the correlation coefficient concerning parameters of length, mass, stiffness, and damping.

4. System response dependency to the main scaling quantities

All inputs in the TTB-2D code have been divided by their respective scales. Then, by calculating the correlation coefficient between the reference response (the system's response to real inputs) and the modified response, charts 3 to 6 have been drawn. The chart for each quantity horizontally increases the scale of that quantity from 2.5 to 25. When scaling each quantity, the scales of other quantities are assumed to be 1. Also, the vertical axis of the charts shows the similarity between the two real and scaled responses. Naturally, at a scale of 1 for each quantity, the correlation value of the real and scaled response will be 1. For this reason, the scales have been examined from 2.5.

According to Figure 3, the correlation chart of the front bogie acceleration response against the change in length scale shows that with an increase in length scale from 2.5 to 25, the correlation coefficient of the front bogie acceleration response decreases from 0.99 to 0.77. This indicates that the length scale has a lesser impact on the correlation chart of the scaled and real responses. Also, the acceleration response of the wagon center against the change in length scale shows a similar trend to the correlation chart of the front bogie acceleration response. Observing similar results for other quantities, it was concluded that the correlation coefficient of the real and scaled responses in the acceleration signal of the front bogie center and the wagon center is the same.

According to Figure 4, the correlation charts of the acceleration response at the center of the front bogie and the wagon center against the change in mass scale also show identical patterns. With an increase in mass scale from 2.5 to 25, the correlation coefficient decreases

from 0.33 to 0 for both the bogie and wagon members. However, with a change in mass scale from 1 to 2.5, the decrease in the correlation coefficient from 1 to 0.33 is observable. This degree of sensitivity indicates that the TTBDI system is very sensitive to changes in mass scale. Also, during construction, parameters related to the mass quantity must be adjusted more precisely.

According to Figure 5, the correlation charts of the acceleration response at the center of the front bogie and the wagon center against the change in stiffness scale show identical patterns. With an increase in stiffness scale from 2.5 to 25, the correlation coefficient decreases from 0.44 to 0.16 for both components. Also, with a change in stiffness scale from 1 to 2.5, the correlation coefficient decreases from 1 to 0.44. These results indicate that the TTBDI system's sensitivity to changes in mass scale is very high, but this sensitivity is less than the sensitivity the system has to mass scale.

According to Figure 6, the correlation charts of the acceleration response at the center of the front bogie and the wagon center against the change in damping coefficient scale show identical patterns. With an increase in the damping coefficient scale from 2.5 to 25, the correlation coefficient decreases from 92% to 70% for both components. This indicates that the damping coefficient scale of the system has a lesser impact on the correlation chart of the scaled and real responses.

5. Method of scaling

In general, the governing differential equations for multi-degree-of-freedom systems' vibrations, after plotting the free-body diagrams for various system components, can be expressed by Equation (20):

$$M\ddot{x}(t) + C\dot{x}(t) + Kx(t) = f(t) \quad (20)$$

The parameters $M\ddot{x}(t)$, $C\dot{x}(t)$, $Kx(t)$, and $f(t)$ must be dimensionally consistent. (The notation [] surrounding each quantity indicates its dimension.)

$$[M\ddot{x}(t)] = [C\dot{x}(t)] = [Kx(t)] = [f(t)] \quad (21)$$

The dimension of displacement is denoted by L, the dimension of velocity is denoted by $\frac{L}{T}$, and the dimension of acceleration is denoted by $\frac{L}{T^2}$. By substituting these variables into Equation (21) Equation (22) will be obtained.

$$[M]\frac{L}{T^2} = [C]\frac{L}{T} = [K]L \quad (22)$$

Equation (23) can be derived by using the variable $\emptyset$.

$$\emptyset_M \frac{\emptyset_L}{{\emptyset_t}^2} = \emptyset_C \frac{\emptyset_L}{\emptyset_t} = \emptyset_K \emptyset_L \quad (23)$$

Given that time is constant in both the scaled and real cases, $\emptyset_t$ is equal to 1, and by eliminating $\emptyset_L$ from both sides of the equation, the result is obtained:

$$\emptyset_M = \emptyset_C = \emptyset_K \quad (24)$$

The obtained result is a crucial finding that has been utilized in scaling. However, the train, track, and bridge system also have another component, which involves using Euler-Bernoulli beams to simulate the bridge and rail. The vibration equation of the Euler-Bernoulli beam is different from the vibration equation of the multi-degree-of-freedom system. In general, the differential equation governing the vibrations of Euler-Bernoulli beams can be expressed as Equation (25):

$$EI\frac{\partial^4 w(x,t)}{\partial x^4} + \mu\frac{\partial^2 w(x,t)}{\partial t^2} = F(x,t) \quad (25)$$

The parameters $EI\frac{\partial^4 w(x,t)}{\partial x^4}$, $\mu\frac{\partial^2 w(x,t)}{\partial t^2}$, and $F(x,t)$ must be dimensionally consistent according to Equation (26). (The notation [] surrounding each quantity indicates its dimension.)

$$\left[EI\frac{\partial^4 w(x,t)}{\partial x^4}\right] = \left[\mu\frac{\partial^2 w(x,t)}{\partial t^2}\right] = [F(x,t)] \quad (26)$$

The dimension of the quantity $w(x,t)$is $\boldsymbol{L}$, and the dimension of $\frac{\partial^4 w(x,t)}{\partial x^4}$ is $\frac{1}{L^3}$.

$$[E][I]\frac{1}{L^3} = [\mu]\frac{L}{T^2} \quad (27)$$

By rewriting Equation (28) using the variable φ, the result can be obtained:

$$\emptyset_E \emptyset_I {\emptyset_L}^{-3} = \emptyset_\mu \frac{\emptyset_L}{{\emptyset_t}^2} \quad (28)$$

Given that time is constant in both the scaled and real cases, ∅_t is equal to 1, and by simplifying Equation (29), the result is obtained.

$$\emptyset_E \emptyset_I = \emptyset_\mu {\emptyset_L}^4 \quad (29)$$

The obtained result is a crucial finding that has been utilized in scaling.

6. Sample case of a scaled example of a train, track, and bridge

Initially, a scaled section is assumed for the beam, with a width of 0.2 meters and a height of 0.001 meters. The second moment of area for the scaled bridge section is obtained in Equation (30), and the ratio of the second moment of area for the section is obtained in Equation (31).

$$I_2 = \frac{1}{12}bh^3 = \frac{1}{12} \times 0.2 \times (0.001)^3 = 1.666 \times 10^{-11} \ \ m^4 \quad (30)$$

$$\emptyset_I = \frac{I_1}{I_2} = \frac{51.3}{1.666 \times 10^{-11}} = \mathbf{30.78 \times 10^{11}} \quad (31)$$

(The subscript 1 corresponds to the actual value of each quantity, and the subscript 2 corresponds to the scaled value of each quantity.)

The chosen material for constructing the bridge is steel, with a modulus of elasticity of 200 GPa and a density of 7850 kg/m^3. By multiplying the density by the cross-sectional area of the bridge (cross-sectional area = 0.2×0.001), the mass per unit length of the bridge is determined to be 1.57 kg/m. Therefore, $\emptyset_E$ and $\emptyset_\mu$ can be deduced.

$$\emptyset_E = \frac{E_1}{E_2} = \frac{35 \times 10^9}{200 \times 10^9} = 0.175 \quad (32)$$

$$\emptyset_\mu = \frac{\mu_1}{\mu_2} = \frac{69000}{1.57} = 43949.044 \quad (33)$$

By substituting the obtained values into Equation (29), the result will be obtained:

$$\emptyset_L = \sqrt[4]{\frac{\emptyset_E \emptyset_I}{\emptyset_\mu}} = \sqrt[4]{\frac{0.175 \times 30.78 \times 10^{11}}{43949.044}} = \sqrt[4]{1.2256 \times 10^7} = 59.16804 \quad (34)$$

Therefore, the length ratio, which represents the scaled dimensions, is equal to 59.16804. From Equation (34), the mass ratio can be

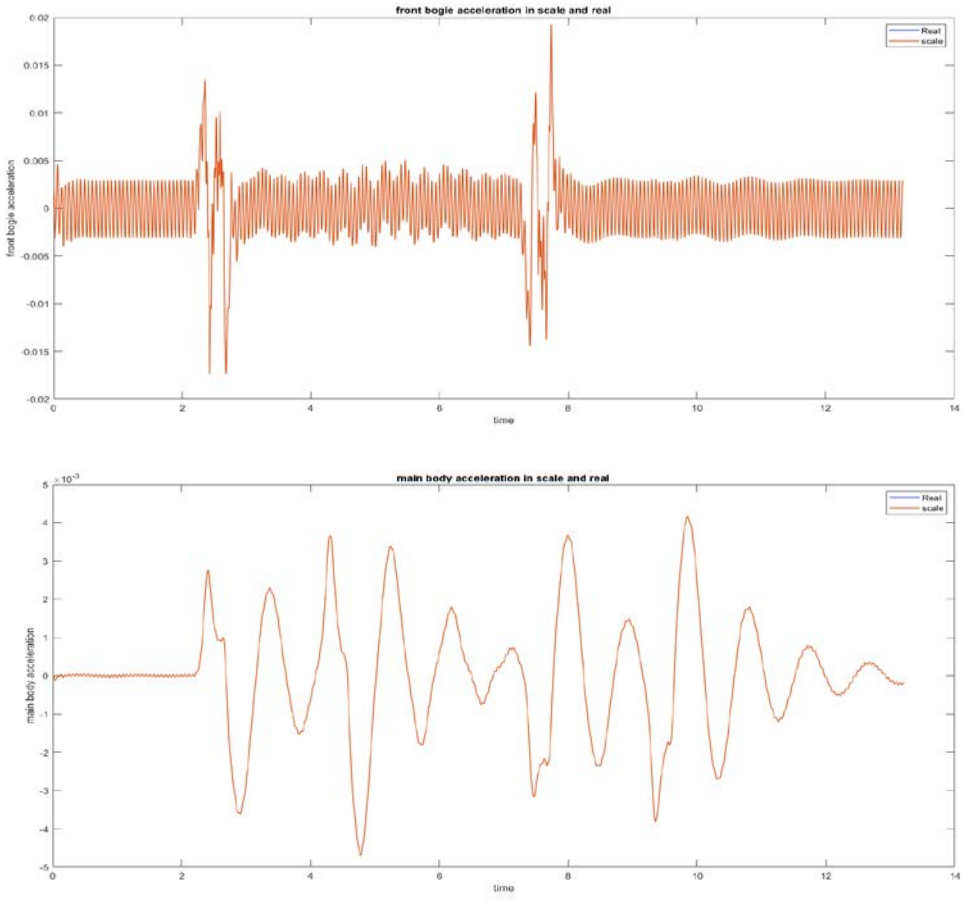

Figure 7. Comparison of the vertical acceleration response of the front bogie and main body in the real response and the scaled response.

determined, which is also equal to the stiffness and damping ratio.

$$\emptyset_\mu = \frac{\emptyset_M}{\emptyset_L} \quad (35)$$

$$43949.044 = \frac{\emptyset_M}{59.16804} \quad (36)$$

$$\emptyset_M = 2600378.7933 \quad (37)$$

Using the scaling factors derived from this scaling method, the simulation response can be compared in two cases: the real response and the scaled response. Figure 7 compares these two responses. It is observed that the response of the TTBDI system to the scaling inputs corresponds to the introduced relations corresponding to the system's response to the actual inputs.

7. Conclusions

The comprehensive analysis presented in this research confirms the effectiveness of dynamic scaling in studying the dynamic interaction of trains, tracks, and bridges. The findings emphasize the importance of precise adjustments in mass-related parameters during the construction of scaled models. The study's methodology ensures that the responses of the scaled TTBDI system closely match those of the actual system. The introduced relationships for dynamic scaling of the train-track-bridge system have been validated. Dynamic scaling devices for train-track-bridge systems are significant because they can simulate various damages and allow for more tests in a shorter time. Consequently, this paper provides a reliable framework for future research in structural health monitoring and damage detection by constructing more accurate dynamic scaling test devices for trains, tracks, and bridges. The established scaling laws and sensitivity assessments pave the way for more precise and efficient neural network training for damage identification in bridge engineering.

References

[1] C. W. Lin and Y. B. Yang, "Use of a passing vehicle to scan the fundamental bridge frequencies: An experimental verification," Eng. Struct., vol. 27, no. 13, pp. 1865–1878, 2005, doi: 10.1016/j.engstruct.2005.06.016.

[2] F. Cerda, S. Chen, J. Bielak, J. H. Garrett, P. Rizzo, and J. KovaČević, "Indirect structural health monitoring of a simplified laboratory-scale bridge model," Smart Struct. Syst., vol. 13, no. 5, pp. 849–868, 2014, doi: 10.12989/sss.2014.13.5.849.

[3] W. Zhang, J. Li, H. Hao, and H. Ma, "Damage detection in bridge structures under moving loads with phase trajectory change of multi-type vibration measurements," Mech. Syst. Signal Process., vol. 87, no. February, pp. 410–425, 2017, doi: 10.1016/j.ymssp.2016.10.035.

[4] C. W. Kim, K. C. Chang, P. J. McGetrick, S. Inoue, and S. Hasegawa, "Utilizing moving vehicles as sensors for bridge condition screening-A laboratory verification," Sensors Mater., vol. 29, no. 2, pp. 153–163, 2017, doi: 10.18494/SAM.2017.1433.

[5] Y. Liu and S. Zhang, "Damage localization of beam bridges using quasi-static strain influence lines based on the BOTDA technique," Sensors (Switzerland), vol. 18, no. 12, 2018, doi: 10.3390/s18124446.

[6] Q. Mei and M. Gül, "A crowdsourcing-based methodology using smartphones for bridge health monitoring," Struct. Heal. Monit., vol. 18, no. 5–6, pp. 1602–1619, 2019, doi: 10.1177/1475921718815457.

[7] S. Zhang and Y. Liu, "Damage detection in beam bridges using quasi-static displacement influence lines," Appl. Sci., vol. 9, no. 9, 2019, doi: 10.3390/app9091805.

[8]Andrzejak, R. G., K. Lehnertz, F. Mormann, C. Rieke, P. David, and C. E. Elger. 2001. "Indications of nonlinear deterministic and finite- dimensional structures in time series of brain electrical activity: Dependence on recording region and brain state." Phys. Rev. E Stat. Nonlin. Soft Matter Phys. 64 (6): 061907. https://doi.org/10.1103/PhysRevE.64.061907.

[9] J. Zhu and Y. Zhang, "Damage Detection in Bridge Structures under Moving Vehicle Loads Using Delay Vector Variance Method," J. Perform. Constr. Facil., vol. 33, no. 5, pp. 1–13, 2019, doi: 10.1061/(asce)cf.1943-5509.0001314.

[10] J. Li, X. Zhu, S. Law, and B. Samali, "Drive-By Blind Modal Identification with Singular Spectrum Analysis," J. Aerosp. Eng., vol. 32, no. 4, p. 04019050, 2019, doi: 10.1061/(asce)as.1943-5525.0001030.

[11] L. Zhang, G. Wu, H. Li, and S. Chen, "Synchronous Identification of Damage and Vehicle Load on Simply Supported Bridges Based on Long-Gauge Fiber Bragg Grating Sensors," J. Perform. Constr. Facil., vol. 34, no. 1, pp. 1–13, 2020, doi: 10.1061/(asce)cf.1943-5509.0001376.

[12] P. J. McGetrick, C. W. Kim, A. González, and E. J. O. Brien, "Experimental validation of a

drive-by stiffness identification method for bridge monitoring," Struct. Heal. Monit., vol. 14, no. 4, pp. 317–331, 2015, doi: 10.1177/1475921715578314.

[13] F. Cerda et al., "Indirect structural health monitoring in bridges: Scale experiments," Bridg. Maintenance, Safety, Manag. Resil. Sustain. - Proc. Sixth Int. Conf. Bridg. Maintenance, Saf. Manag., pp. 346–353, 2012.

[14] G. Lederman et al., "Damage quantification and localization algorithms for indirect SHM of bridges," Bridg. Maintenance, Safety, Manag. Life Ext. - Proc. 7th Int. Conf. Bridg. Maintenance, Saf. Manag. IABMAS 2014, no. July, pp. 640–647, 2014, doi: 10.1201/b17063-93.

[15] C. W. Kim, R. Isemoto, P. J. Mcgetrick, M. Kawatani, and E. J. Obrien, "Drive-by bridge inspection from three different approaches," Smart Struct. Syst., vol. 13, no. 5, pp. 775–796, 2014, doi: 10.12989/sss.2014.13.5.775.

[16] J. Zhang, D. Yang, W. X. Ren, and Y. Yuan, "Time-varying characteristics analysis of vehicle-bridge interaction system based on modified S-transform reassignment technique," Mech. Syst. Signal Process., vol. 160, p. 107807, 2021, doi: 10.1016/j.ymssp.2021.107807.

[17] Z. Nie, J. Lin, J. Li, H. Hao, and H. Ma, "Bridge condition monitoring under moving loads using two sensor measurements," Struct. Heal. Monit., vol. 19, no. 3, pp. 917–937, 2020, doi: 10.1177/1475921719868930.

[18] S. Pourzeynali, X. Zhu, A. G. Zadeh, M. Rashidi, and B. Samali, "Comprehensive study of moving load identification on bridge structures using the explicit form of newmark-β method: Numerical and experimental studies," Remote Sens., vol. 13, no. 12, 2021, doi: 10.3390/rs13122291.

[19] D. Cantero, P. McGetrick, C. W. Kim, and E. OBrien, "Experimental monitoring of bridge frequency evolution during the passage of vehicles with different suspension properties," Eng. Struct., vol. 187, no. January, pp. 209–219, 2019, doi: 10.1016/j.engstruct.2019.02.065.

[20] S. Urushadze and J. D. Yau, "Experimental Verification of Indirect Bridge Frequency Measurement Using a Passing Vehicle," Procedia Eng., vol. 190, pp. 554–559, 2017, doi: 10.1016/j.proeng.2017.05.379.

[21] D. …… …… Fracture of Engineering Materials & Structures, Vol.1, No.3, (2002), pp.899-909.

[23] Nguyen K, Goicolea JM, Galbadon F. Comparison of dynamic effects of high-speed traffic load on ballasted track using a simplified two-dimensional and full three-dimensional model. Proc Inst Mech Eng 2014;2228(2):128–42. http://dx.doi.org/10.1177/F0954409712465710.

[24] European Rail Research Institute. Rail Bridges for Speeds > 200 km/h. 1999, Train-bridge interaction (ERRI D214/RP 4).

[25] Quirke P, Bowe C, OBrien EJ, Cantero D, Antolin P, Goicolea JM. Railway bridge damage detection using vehicle-based inertial measurements and apparent profile. Eng Struct 2017;153:421–42. http://dx.doi.org/10.1016/j. engstruct.2017.10.023.

[26] Ren Y, OBrien EJ, Cantero D, Keenahan J. Railway bridge condition moni- toring using numerically calculated responses from batches of trains. Appl Sci 2022;12:4972. http://dx.doi.org/10.3390/app12104972.

[27]Handbook of Railway Vehicle Dynamics, Simon Iwnicki, Maksym Spiryagin, Colin Cole, Tim McSweeney, CRC Press Taylor & Francis Group 6000 Broken Sound Parkway NW, Suite 300 Boca Raton, FL 33487-2742,2020

[28]https://en.wikipedia.org/wiki/Pearson_correlation_coefficient

Appendix

Table 2. Train dynamic and geometric data

Variable	Description	value	unit
V	Speed of train	10	$\frac{m}{s}$
m	Main body mass	32000	Kg
I_v	Main body moment of inertia	1970000	$Kg.m^2$
L_v	Main body length (axle to axle)	19	m
L_F	Additional front length	3	m
L_B	Additional back length	3	m
m_{Bi}	Mass of i-th bogie	2615	Kg
I_{Bi}	Moment of inertia of i-th bogie	1476	$Kg.m^2$
L_{Bi}	Bogie length	2.56	m
m_w	Total mass of i-th axle and wheels	1813	Kg
K_{pi}	Primary suspension vertical stiffness of i-th axle	2400000	$\frac{N}{m}$
C_{pi}	Primary suspension vertical viscous damping of i-th axle	8000	$\frac{N.s}{m}$
K_{si}	Secondary suspension vertical stiffness of i-th axle	860000	$\frac{N}{m}$
C_{si}	Secondary suspension vertical viscous damping of i-th axle	40000	$\frac{N.s}{m}$

Table 3. Dynamic and geometric data of track and bridge

Variable	Description	value	unit
E_R	Young's modulus of rail material	2.059e11	$\frac{N}{m^2}$
J_R	Rail section's second moment of area	6.434e-5	m^4
μ_R	Mass per unit length of rail	61.28	$\frac{Kg}{m}$
K_P	Vertical stiffness of pad	6.5e7	$\frac{N}{m}$
C_P	Vertical viscous damping of pad	7.5e4	$\frac{N.s}{m}$
L_S	Distance between sleepers	0.6	m
m_S	Mass of each sleeper	251	Kg
m_{BA}	Mobilized ballast mass	531.4	Kg
K_{BA}	Ballast vertical stiffness	137.75e6	$\frac{N}{m}$
C_{BA}	Ballast vertical viscous damping	5.88e4	$\frac{N.s}{m}$
K_{SB}	Primary suspension vertical stiffness of i-th axle	77.5e6	$\frac{N}{m}$
C_{SB}	Sub-ballast vertical viscous damping	3.115e4	$\frac{N.s}{m}$
L	Bridge span	50	m
E	Modulus of elasticity	35e9	$\frac{N}{m^2}$
J	Section's second moment of area	51.3	m^4
μ	Mass per unit length of bridge	69000	$\frac{Kg}{m}$
η	Damping ratio per unit length of bridge	1	%